

Conservative, special-relativistic smooth particle hydrodynamics

Stephan Rosswog

School of Engineering and Science, Jacobs University Bremen, 28759 Bremen, Germany

Abstract

We derive a new special-relativistic version of Smooth Particle Hydrodynamics (SPH) from the Lagrangian of an ideal fluid. The new formulation accounts for the terms that stem from non-constant smoothing lengths, in SPH usually called "grad-h terms". To handle shocks a refined artificial viscosity scheme is applied. The performance of this new equation set is explored in a variety of benchmark tests and the results of the new formulation are compared against an earlier special-relativistic SPH version. The new approach generally yields excellent results. As expected from a Lagrangian method, it performs extremely well in supersonic advection tests, but also for strong relativistic shocks, usually considered a particular challenge for SPH, the method yields convincing results. It is, for example, able to handle Lorentz-factors as large as $\gamma = 50\,000$ in the so-called wall shock test.

Key words: computational fluid dynamics, shocks, special relativity, smooth particle hydrodynamics

1 Introduction

Special-relativistic hydrodynamics has important applications in the fields of heavy ion collisions and in astrophysics. Astrophysical examples include jets from Active Galactic Nuclei [6], pulsar winds [15] or gamma-ray bursts [35] and often involve Lorentz factors substantially in excess of $\gamma = 10$. Analytical solutions are only known for a small set of specific problems, for most relevant cases numerical approaches are required. A robust special-relativistic scheme can be directly applied to problems of the above type and, in addition, it can serve as an essential ingredient of a general-relativistic code, a tool that opens up the possibility to tackle a whole new class of interesting astrophysical questions.

In recent years, grid-based methods for special-relativistic hydrodynamics have

seen a huge leap forward, and by now many highly accurate Eulerian schemes exist, see [26] for a review. Most of these schemes are fine-tuned to solve 1D relativistic shock problems without oscillations and with sharp discontinuities. For many astrophysical problems, however, further capabilities such as the accurate advection of smooth flow features are required. In particular, for some of the future applications that we have in mind a purely Lagrangian method possesses distinct advantages and that is why we focus in this paper on a refined special-relativistic formulation of the Smooth Particle Hydrodynamics (SPH) method.

SPH is a Lagrangian, purely mesh-free particle method. Since its first formulations in an astrophysical context [20,16] SPH has undergone a slew of technical improvements and it has found its way into many other branches of computationally oriented areas of science. For reviews of the method see [4,27,30,37]. Being entirely Lagrangian, the method has obvious advantages in advection problems, on the other hand, strong shocks have traditionally posed serious challenges. Our aim is to devise a special-relativistic SPH formulation that, at least at decent resolution, yields accurate shock-results while keeping the other benefits of a Lagrangian scheme. This formulation is intended to become the condensation nucleus for a future, fixed-metric implementation of general relativistic SPH.

The paper is organized as follows. In Section 2 we derive an SPH form of the special-relativistic equations of an ideal fluid that includes corrective terms from gradients of the SPH smoothing kernel with respect to the resolution length. In Section 3 we investigate the performance of the new equation set in a number of special-relativistic benchmark tests. Section 4 summarizes the main results.

2 Special-relativistic SPH with grad-h terms

In the SPH discretization process, derivatives are expressed as sums over particle properties, weighted with the gradient of a smoothing kernel whose width is determined by the so-called smoothing length. If symmetrized appropriately, the SPH-discretized fluid equations conserve mass, energy, linear and angular momentum by construction. In early SPH formulations the derivatives of the kernel functions with respect to the smoothing length were assumed to vanish. In practice, however, the smoothing lengths were still evolved to ensure a local adaptivity of the method and this inconsistency lead to a violation of the conservation properties. How severe this violation is in practice, depends on the considered problem [41,36,38]. This deficiency was first addressed by [33] and, more recently, by [41] and [27] who derived the SPH equations from a discretized fluid Lagrangian. The latter two formulations result in multiplicative correction terms, the so-called “grad-h terms”. The SPH method has

also been applied to relativistic problems [17,21,22,18,7,40], but none of these approaches included grad-h terms.

Here we follow the approach of [31] and derive the special-relativistic SPH equations from a variational principle, but we also account for the kernel derivatives with respect to the smoothing length. For the flat-space metric tensor, $\eta_{\mu\nu}$, we use the signature $(-,+,+,+)$, Latin indices run over $(1,2,3)$, Greek ones run from 0 to 3 with the zero component being time. We apply the Einstein sum convention and use $c = 1$ unless otherwise noted. With these conventions the four-velocity, $U^\mu = dx^\mu/d\tau$ is normalized to $U_\mu U^\mu = -1$.

2.1 The Lagrangian

The Lagrangian of a perfect fluid can be written as [14]

$$L_{\text{pf,sr}} = - \int T^{\mu\nu} U_\mu U_\nu dV, \quad (1)$$

where

$$T^{\mu\nu} = (n[1 + u(n, s)] + P)U^\mu U^\nu + P\eta^{\mu\nu} \quad (2)$$

denotes the energy momentum tensor, n is the baryon number density in the local fluid rest frame, u is the thermal energy per baryon, s the specific entropy and P the pressure. All these quantities are measured in the local rest frame of each fluid element, energies are measured in units of the baryon rest mass energy, $m_0 c^2$ ¹. By using the normalization of the four-velocity, the Lagrangian simplifies to

$$L_{\text{pf,sr}} = - \int n(1 + u) dV. \quad (3)$$

In the general case, a fluid element moves with respect to the frame in which the computations are performed (“computing frame”, CF). Therefore, the baryon number density in the CF, N , is related to the local fluid rest frame via a Lorentz contraction

$$N = \gamma n, \quad (4)$$

where γ is the Lorentz factor of the fluid element as measured in the CF. The simulation volume in the CF can be subdivided into volume elements such

¹ The appropriate mass m_0 obviously depends on the ratio of neutrons to protons, i.e. on the nuclear composition of the considered fluid.

that each element b contains ν_b baryons

$$\Delta V_b = \frac{\nu_b}{N_b}. \quad (5)$$

These volume elements are used in the SPH discretization process to approximate a quantity f given at a set of discrete points (“particles”) labelled by b :

$$f(\vec{r}) = \sum_b f_b \frac{\nu_b}{N_b} W(|\vec{r} - \vec{r}_b|, h), \quad (6)$$

where our notation does not distinguish between the approximated values (the f on the LHS) and the values at the particle positions (f_b on the RHS). The quantity h is the smoothing length that characterizes the width of the smoothing kernel W , for which we use a cubic spline kernel [27,30]. The discretization prescription, Eq. (6), yields for the baryon number density in the computing frame:

$$N(\vec{r}) = \sum_b \nu_b W(|\vec{r} - \vec{r}_b|, h). \quad (7)$$

This equation takes over the role of the usual density summation of non-relativistic SPH, $\rho(\vec{r}) = \sum_b m_b W(|\vec{r} - \vec{r}_b|, h)$. Since we keep the baryon numbers associated with each SPH particle, ν_b , fix, there is no need to evolve a continuity equation and baryon number is conserved by construction. If desired, the continuity equation can be solved though, see e.g. [7]. The discretized fluid Lagrangian reads

$$L_{\text{SPH,sr}} = - \sum_b \frac{\nu_b}{N_b} n_b [1 + u(n_b, s_b)], \quad (8)$$

or, by use of Eq. (4)

$$L_{\text{SPH,sr}} = - \sum_b \frac{\nu_b}{\gamma_b} [1 + u(n_b, s_b)]. \quad (9)$$

2.2 The momentum equation

The momentum evolution of a particle a follows from the Euler-Lagrange equations

$$\frac{d}{dt} \frac{\partial L_{\text{SPH,sr}}}{\partial \vec{v}_a} - \frac{\partial L_{\text{SPH,sr}}}{\partial \vec{v}_a} = 0. \quad (10)$$

In calculating the baryon number density of particle, b , we use b 's own smoothing length

$$N_b = \sum_k \nu_k W(|\vec{r}_b - \vec{r}_k|, h_b) \quad (11)$$

and adapt the smoothing length according to

$$h_b = \eta N_b^{-1/D}, \quad (12)$$

where η is a suitably chosen numerical constant, usually in the range between 1.3 and 1.5, and D is the number of spatial dimensions. Hence, similar to the non-relativistic case [41,29], the density and the smoothing length mutually depend on each other and an iteration is required to obtain a self-consistent solution for both. The density gradient with respect to particle position a is given by

$$\begin{aligned} \nabla_a N_b &= \sum_k \nu_k \left(\frac{\partial W_{bk}(h_b)}{\partial r_{bk}} \frac{\partial r_{bk}}{\partial \vec{r}_a} + \frac{\partial W_{bk}(h_b)}{\partial h_b} \frac{\partial h_b}{\partial N_b} \frac{\partial N_b}{\partial \vec{r}_a} \right) \\ &= \frac{1}{\tilde{\Omega}_b} \sum_k \nu_k \nabla_b W_{bk}(h_b) (\delta_{ba} - \delta_{ka}), \end{aligned} \quad (13)$$

where the ‘‘grad-h’’ correction factor

$$\tilde{\Omega}_b \equiv 1 - \frac{\partial h_b}{\partial N_b} \sum_k \frac{\partial W_{bk}(h_b)}{\partial h_b} \quad (14)$$

was introduced. Similarly, the time derivative becomes

$$\begin{aligned} \frac{dN_a}{dt} &= \sum_b \nu_b \left(\frac{\partial W_{ab}(h_a)}{\partial r_{ab}} \frac{dr_{ab}}{dt} + \frac{\partial W_{ab}(h_a)}{\partial h_a} \frac{\partial h_a}{\partial N_a} \frac{dN_a}{dt} \right) \\ &= \frac{1}{\tilde{\Omega}_a} \sum_b \nu_b \vec{v}_{ab} \nabla_a W_{ab}(h_a). \end{aligned} \quad (15)$$

The canonical momentum is given by

$$\vec{p}_a \equiv \frac{\partial L_{\text{SPH,SR}}}{\partial \vec{v}_a} = - \sum_b \nu_b \frac{\partial}{\partial \vec{v}_a} \left(\frac{1 + u(n_b, s_b)}{\gamma_b} \right) = \nu_a \gamma_a \vec{v}_a \left(1 + u_a + \frac{P_a}{n_a} \right) \quad (16)$$

where we have used the first law of thermodynamics,

$$\left(\frac{\partial u_b}{\partial n_b} \right)_s = \frac{P_b}{n_b^2} \quad (17)$$

and the relation between the baryon number densities in the different frames, Eq. (4). The last term in brackets on the RHS of Eq. (16) is the enthalpy per baryon. We numerically evolve the relativistic canonical momentum per baryon,

$$\vec{S}_a \equiv \gamma_a \vec{v}_a \left(1 + u_a + \frac{P_a}{n_a} \right). \quad (18)$$

To find its evolution equation $\partial L / \partial \vec{r}_a$ needs to be calculated. By once more using the chain rule, the first law of thermodynamics, Eq. (17), Eq. (4), Eq. (13) and $\nabla_b W_{ba} = -\nabla_a W_{ab}$, which follows from the choice of a radial kernel, $W(\vec{r}) = W(|\vec{r}|)$, one finds

$$\begin{aligned} \frac{\partial L_{\text{SPH,SR}}}{\partial \vec{r}_a} &= - \sum_b \frac{\nu_b}{\gamma_b} \frac{\partial u_b}{\partial \vec{r}_a} = - \sum_b \frac{\nu_b}{\gamma_b^2} \frac{P_b}{n_b^2} \nabla_a N_b \\ &= -\nu_a \sum_b \nu_b \left(\frac{P_a}{N_a^2 \tilde{\Omega}_a} \nabla_a W_{ab}(h_a) + \frac{P_b}{N_b^2 \tilde{\Omega}_b} \nabla_a W_{ab}(h_b) \right), \end{aligned} \quad (19)$$

so that the special-relativistic momentum equation reads

$$\frac{d\vec{S}_a}{dt} = - \sum_b \nu_b \left(\frac{P_a}{N_a^2 \tilde{\Omega}_a} \nabla_a W_{ab}(h_a) + \frac{P_b}{N_b^2 \tilde{\Omega}_b} \nabla_a W_{ab}(h_b) \right). \quad (20)$$

2.3 The energy equation

We use the canonical energy to identify a suitable energy variable

$$E \equiv \sum_a \frac{\partial L}{\partial \vec{v}_a} \cdot \vec{v}_a - L = \sum_a \nu_a \left(\vec{v}_a \cdot \vec{S}_a + \frac{1 + u_a}{\gamma_a} \right), \quad (21)$$

which can be transformed into

$$E = \sum_a \nu_a \left[\gamma_a \left(1 + u_a + \frac{P_a}{n_a} \right) - \frac{P_a}{N_a} \right]. \quad (22)$$

As numerical energy variable we choose the canonical energy per baryon

$$\epsilon_a \equiv \gamma_a \left(1 + u_a + \frac{P_a}{n_a} \right) - \frac{P_a}{N_a} = \vec{v}_a \cdot \vec{S}_a + \frac{1 + u_a}{\gamma_a}. \quad (23)$$

By using Eq. (4) once more one finds

$$\frac{d}{dt} \left(\frac{1 + u_a}{\gamma_a} \right) = \frac{P_a}{N_a^2} \frac{dN_a}{dt} - \vec{S}_a \cdot \frac{d\vec{v}_a}{dt} \quad (24)$$

and therefore

$$\frac{d\epsilon_a}{dt} = \frac{d}{dt} \left\{ \vec{v}_a \cdot \vec{S}_a + \frac{1 + u_a}{\gamma_a} \right\} = \vec{v}_a \cdot \frac{d\vec{S}_a}{dt} + \frac{P_a}{N_a^2} \frac{dN_a}{dt}. \quad (25)$$

By inserting Eqs. (15) and (20) into (25), the energy equation becomes

$$\frac{d\epsilon_a}{dt} = - \sum_b \nu_b \left(\frac{P_a \vec{v}_b}{N_a^2 \tilde{\Omega}_a} \cdot \nabla_a W_{ab}(h_a) + \frac{P_b \vec{v}_a}{N_b^2 \tilde{\Omega}_b} \cdot \nabla_a W_{ab}(h_b) \right), \quad (26)$$

similar to the non-relativistic case when the "thermokinetic energy" $\frac{1}{2}v^2 + u$ is evolved, e.g. [30].

2.4 Artificial dissipation

Usually artificial viscosity is used in SPH to handle shocks. Guided by the successes of relativistic Riemann solvers [24], Monaghan has constructed a new form of artificial viscosity terms [28]. The idea is not to implement Riemann solvers into SPH, but instead to devise a robust shock treatment scheme that does not require the restriction to an ideal gas and that avoids the explicit solution of the Riemann problem.

2.4.1 The form of the dissipative terms

The dissipative terms used in this work are similar to the suggestion of Chow and Monaghan [7]

$$\left(\frac{d\vec{S}_a}{dt} \right)_{\text{diss}} = - \sum_b \nu_b \Pi_{ab} \overline{\nabla_a W_{ab}} \quad \text{with} \quad \Pi_{ab} = - \frac{K v_{\text{sig}}}{\bar{N}_{ab}} (\vec{S}_a^* - \vec{S}_b^*) \cdot \hat{e}_{ab} \quad (27)$$

and

$$\left(\frac{d\epsilon_a}{dt} \right)_{\text{diss}} = - \sum_b \nu_b \Omega_{ab} \overline{\nabla_a W_{ab}} \quad \text{with} \quad \Omega_{ab} = - \frac{K v_{\text{sig}}}{\bar{N}_{ab}} (\epsilon_a^* - \epsilon_b^*) \hat{e}_{ab}. \quad (28)$$

Here K is a numerical constant of order unity, v_{sig} an appropriately chosen signal velocity, see below, $\bar{N}_{ab} = (N_a + N_b)/2$, and

$$\hat{e}_{ab} = \frac{\vec{r}_a - \vec{r}_b}{|\vec{r}_a - \vec{r}_b|} \quad (29)$$

is the unit vector pointing from particle b to particle a . For the symmetrized kernel gradient we use

$$\overline{\nabla_a W_{ab}} = \frac{1}{2} [\nabla_a W_{ab}(h_a) + \nabla_a W_{ab}(h_b)]. \quad (30)$$

Note that in [7] $\nabla_a W_{ab}(h_{ab})$ was used instead of $\overline{\nabla_a W_{ab}}$, in practice we find the differences between the two symmetrizations negligible. The stars at the variables in Eqs. (27) and (28) indicate that the projected Lorentz factors

$$\gamma_k^* = \frac{1}{\sqrt{1 - (\vec{v}_k \cdot \hat{e}_{ab})^2}} \quad (31)$$

are used instead of the normal Lorentz factor in Eq. (18) and (23). This projection onto the line connecting particle a and b has been chosen to guarantee that the viscous dissipation is positive definite [7].

2.4.2 Signal velocity

The signal velocity that enters the artificial dissipation terms is an estimate for the speed of approach of a signal sent from particle a to particle b . The idea is to have a physically sound estimate that does not require much computational effort. In [28,7] the numerical solution of test problems was found to be rather insensitive to the exact form of v_{sig} . For our formulation, we use

$$v_{\text{sig,ab}} = \max(\alpha_a, \alpha_b), \quad (32)$$

where

$$\alpha_k^\pm = \max(0, \pm \lambda_k^\pm) \quad (33)$$

with λ_k^\pm being the extreme local eigenvalues of the Euler equations

$$\lambda_k^\pm = \frac{v_k \pm c_{s,k}}{1 \pm v_k c_{s,k}} \quad (34)$$

and $c_{s,k}$ being the relativistic sound velocity of particle k . These 1D estimates can be generalized to higher spatial dimensions [26]. The results are not particularly sensitive to the exact form of the signal velocity, but in experiments we find that Eq. (32) yields somewhat crisper shock fronts and less smeared contact discontinuities (for the same value of K) than the suggestions of [7].

2.4.3 Controlling the amount of dissipation

The ultimate aim of artificial dissipative terms is to make “discontinuities” numerically treatable by smoothing them over a few resolution lengths. Away from the locations where they are required, such terms should be ineffective, or, ideally, they should be absent. To achieve this we follow the idea of time-dependent dissipation parameters [32]. Instead of a constant dissipation parameter K in Eqs. (27) and (28) we use time-dependent values $K = \min(K_{\max}, K(t))$, where $K(t) = 0.5[K_a(t) + K_b(t)]$ and each particle’s parameter is evolved according to

$$\frac{dK_k}{dt} = S_k - \frac{K_k(t) - K_{\min}}{\tau_k}. \quad (35)$$

The particle’s source term S_k leads to a rise of K , if S_k is negligible, K decays to a minimum value, K_{\min} on a time scale τ_k . For the decay time we choose

$$\tau_a = \frac{\chi h_a}{\min_b(v_{\text{sig},ab})}, \quad (36)$$

where χ is a numerical parameter. The source term, S_k , should trigger on regions where artificial dissipation is desirable, namely near the shock front and near the contact discontinuity. To achieve this, we choose two different source terms. The first,

$$S_{k,s} = \frac{1}{N_k} \max\left(0, \frac{dN_k}{dt}\right), \quad (37)$$

triggers on compression to detect shocks, the second,

$$S_{k,\text{cd}} = \kappa \left| \frac{d^2(u_k \gamma_k)}{dx^2} \right| \frac{h_k}{\min_b(v_{\text{sig},kb})}, \quad (38)$$

triggers on second derivatives of the internal energy (as measured in the CF) which are calculated as in [5]. The final source term used reads

$$S_k = \max(S_{k,s}, S_{k,\text{cd}}). \quad (39)$$

This source term has performed well in the presented tests, but other choices are certainly possible and there may be room for improvement. The numerical parameters, K_{\max} , K_{\min} , χ and κ , could be tuned to reach optimal results for each test. This, however, is only possible if an exact solution is known and instead of such a fine tuning approach we search a set of parameters that can robustly reproduce the known results. Unless otherwise noted, we use $K_{\max} = 0.5$, $K_{\min} = 0.01$, $\chi = 5$ and $\kappa = 10$. This value of K_{\max} was also used in [7] and therefore allows for a fair comparison with their results.

2.5 Conversion between primitive and numerical variables

At the end of a time step the physical quantities γ , u , n and v need to be calculated from the updated numerical quantities N , \vec{S} and ϵ . We follow the strategies of earlier special-relativistic approaches [25,28]: all variables in the (polytropic) equation of state

$$P = (\Gamma - 1)nu \tag{40}$$

are expressed as a function of the updated numerical variables and the pressure itself. The resulting equation is solved numerically for the new pressure which is subsequently used to recover the physical variables. From Eq. (18) and (23) one finds

$$\vec{v} = \frac{\vec{S}}{\epsilon + P/N} \tag{41}$$

and thus

$$\gamma = \frac{1}{\sqrt{1 - S^2/(\epsilon + P/N)^2}}. \tag{42}$$

Using Eq. (41) and Eq. (4) one can express the specific energy as

$$u = \frac{\epsilon}{\gamma} + \frac{P}{\gamma N}(1 - \gamma^2) - 1. \tag{43}$$

With aid of Eqs. (4) and (43) Eq. (40) can be solved for the new pressure P that corresponds to the new values of the integrated numerical variables. Once P is known, the Lorentz factor can be calculated from Eq. (42), the specific energy from Eq. (43) and the velocity from Eq. (41).

3 Reference formulation

The performance of the new equation set is compared to the formulation of [7] which produces the best shock test results of all published SPH formulations that we are aware of²

$$N_a = \sum_b \nu_b W_{ab}(h_{ab}) \quad (44)$$

$$\frac{d\vec{S}_a}{dt} = - \sum_b \nu_b \left(\frac{P_a}{N_a^2} + \frac{P_b}{N_b^2} + \Pi_{ab,\text{CM}} \right) \nabla_a W_{ab}(h_{ab}) \quad (45)$$

$$\frac{d\epsilon_a}{dt} = - \sum_b \nu_b \left(\frac{P_a \vec{v}_b}{N_a^2} + \frac{P_b \vec{v}_a}{N_b^2} + \Omega_{ab,\text{CM}} \right) \cdot \nabla_a W_{ab}(h_{ab}), \quad (46)$$

where $h_{ab} = (h_a + h_b)/2$ and

$$\Pi_{ab,\text{CM}} = \frac{K v_{\text{sig}}}{N_{ab}} (\vec{S}_a^* - \vec{S}_b^*) \cdot \hat{e}_{ab} \quad \text{and} \quad \Omega_{ab,\text{CM}} = \frac{K v_{\text{sig}}}{N_{ab}} (\epsilon_a^* - \epsilon_b^*) \hat{e}_{ab}, \quad (47)$$

where they use a fixed value $K = 0.5$. For the following comparisons we use their first suggestion for the signal velocity

$$v_{\text{sig,CM}} = \frac{c_a + |v_{ab}^*|}{1 + c_a |v_{ab}^*|} + \frac{c_b + |v_{ab}^*|}{1 + c_b |v_{ab}^*|} + |v_{ab}^*|, \quad \text{where} \quad v_{ab}^* = -\vec{v}_{ab} \cdot \hat{e}_{ab}, \quad (48)$$

their suggested alternative yields very similar results [7].

4 Numerical results

We use equal mass particles in our tests, so that the density information is encoded in the particle separation. Consistent with SPH's property of smoothing discontinuities over ~ 3 smoothing lengths, we approximate discontinuities in the initial conditions of a function f via Fermi-functions

$$f(x) = \frac{f_L - f_R}{1 + \exp\left(\frac{x-x_S}{\Delta x}\right)} + f_R, \quad (49)$$

where f_L and f_R are the values to the left and right of the discontinuity located at x_S and Δx is the characteristic transition length. We typically use

² Note that [7] obtain the density from integration, but the difference is negligible.

the average of the left and right interparticle separation for Δx . The equations are integrated with a third-order Runge-Kutta-Fehlberg method, energy and momentum are conserved to about one part in 10^{14} . Unless otherwise noted, about 3000 particles are shown and a polytropic equation of state with an adiabatic exponent specific to each test is used.

4.1 Test 1: mildly relativistic shock tube

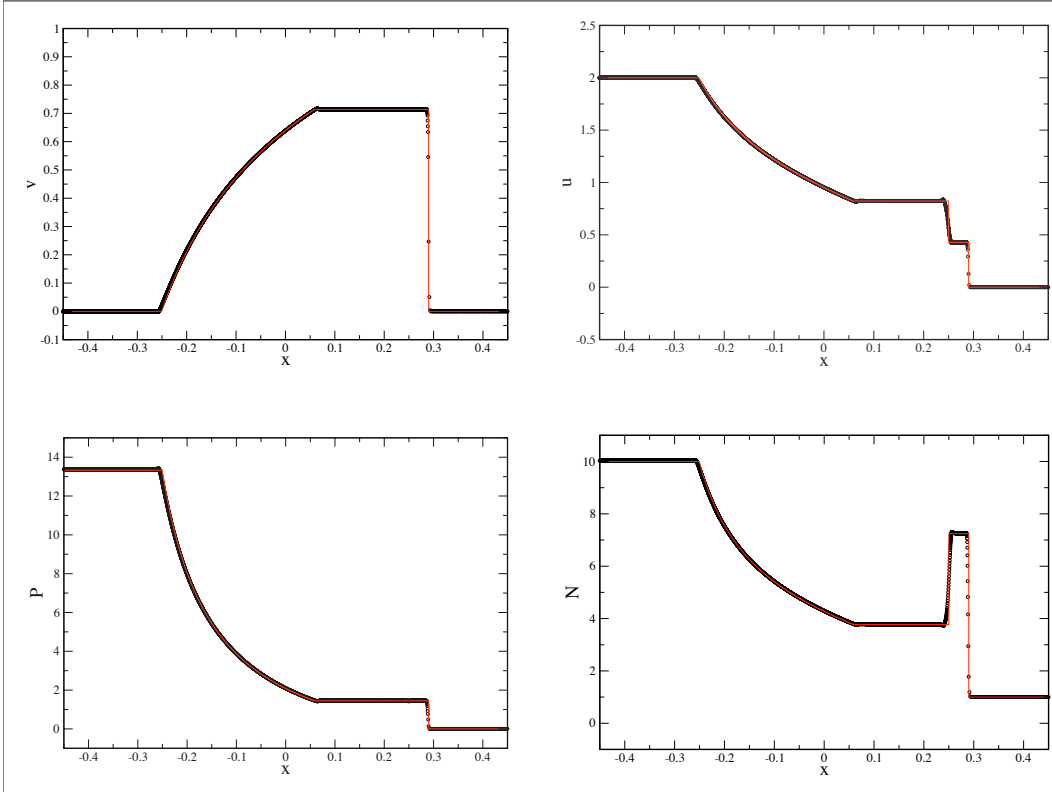


Fig. 1. Mildly relativistic shock tube [26] at $t=0.35$: velocity (in units of the speed of light; upper left), thermal energy (upper right), pressure (lower left) and computing frame number density (lower right). The SPH solution is shown as black circles, the exact solution as the red line.

This mildly relativistic shock tube ($\gamma_{\max} \approx 1.4$) has become a widespread benchmark for relativistic hydrodynamics codes [25,7,39,8,26]. It uses a polytropic exponent of $\Gamma = 5/3$, vanishing initial velocities everywhere, the left state has a pressure $P_L = 40/3$ and a density $N_L = 10$, while the right state is prepared with $P_R = 10^{-6}$ and $N_R = 1$.

The SPH result (circles, at $t=0.35$) agrees excellently with the exact solution (solid line), see Fig. 1. Only the contact discontinuity at $x \approx 0.25$ is somewhat smeared out. A striking difference to earlier SPH results [18,40] is the absence of any spike in u and P at the contact discontinuity. This is a result of both the resolvable, initial discontinuity and, more importantly, of the form of the

dissipative terms, Eqs. (27) and (28).

To explore the dependence of the results on the various new elements we perform the following low-resolution (400 particles between -0.3 and 0.3) runs: i) use the new equation set, ii) the reference equation set of Chow and Monaghan [7] iii) the new equation set, but $\Omega = 1$ to explore the importance of the “grad-h”-terms and iv) the new equation set, but $K = K_{\max} = 0.5$ to explore the effect of the time-dependent viscosity parameters. The results are displayed in Fig. 2. All numerical parameters have exactly the same values in all cases. Generally we find a good agreement between the different equation sets. For a comparison we show the density N since the shock-compressed shell is difficult to capture and therefore shows the strongest deviations from the exact solution. The ”grad-h” terms improve the left edge of the rarefaction

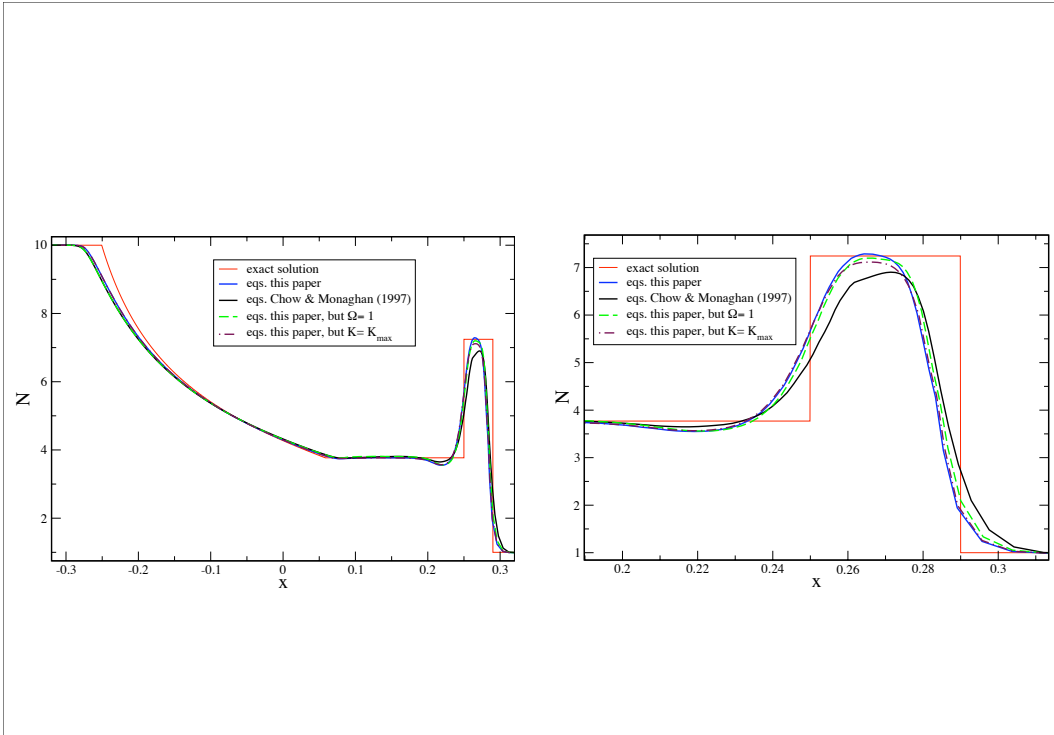


Fig. 2. Comparison of three different equation sets (at very low resolution): the equation set of this paper (red), the equations of this paper, but Ω_a set to unity, and the equation set of Chow & Monaghan (1997).

fan and increase the density peak in the shock-compressed shell (solid blue vs. dashed green). The time-dependent viscosity parameters are substantially reduced behind the shock which further enhances this tendency (solid blue vs. dot-dashed maroon). The main difference between the suggested and the reference equation set seem to come from the use of the different signal velocity, the grad-h terms are only a minor improvement.

4.2 Test 2: strong blast

The following test with initial conditions $(\rho, v, P)^L = (1, 0, 1000)$ and $(\rho, v, P)^R = (1, 0, 0.01)$ is a more relativistic variant of a shock tube and was first considered by [34]. It poses a severe challenge since relativistic effects compress the post-shock state into a very thin and dense shell. The fluid in the shell moves at a velocity of $v = 0.96$ which corresponds to a Lorentz factor of $\gamma_{\text{shell}} = 3.6$, the shock front moves with a velocity of 0.986, i.e. $\gamma_{\text{shock}} = 6.0$. This test has become a standard benchmark for relativistic schemes [34,11,24,23,25,13,43,7,10,8,3,26]. Overall, the numerical solution (shown at $t=0.16$) agrees well with the exact

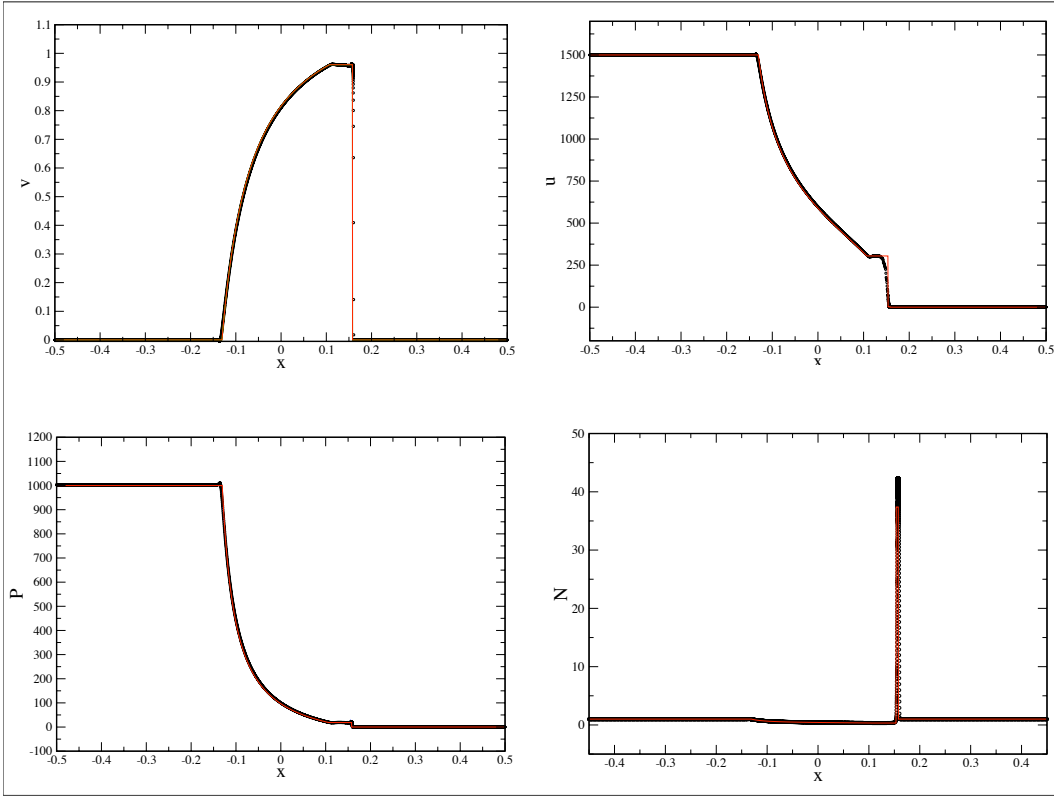


Fig. 3. Strong blast [26]: velocity (in units of the speed of light; upper left), thermal energy (upper right), pressure (lower left) and computing frame number density (lower right). The SPH solution is shown as black circles, the exact solution as the red line.

one, see Fig. 3. In particular, the intermediate states in velocity and pressure are well-captured. However, this difficult test is a severe challenge and the numerical solution is not free of deficiencies. Somewhat large smearing in the internal energy occurs at $x \approx 0.15$, this is a result of using the maximum local eigenvalues rather than a proper spectral decomposition. Also, the numerical peak density value exceeds the exact one and the shock moves at a slightly too large velocity, effects that decrease with increasing numerical resolution. In comparison to [7] both these artifacts are substantially reduced, but nev-

ertheless still present.

We again perform a set of test runs (400 particles between -0.5 and 0.5): i) use the new suggested equation set, ii) the reference equation set of Chow and Monaghan [7] iii) the new suggested equation set, but $\Omega = 1$ to explore the importance of the “grad-h”-terms and iv) the new equation set, but $K = K_{\max} = 0.5$ to explore the effect of the time-dependent viscosity parameters. The results are displayed in Fig. 4 together with a zoom-in from the calculation shown in Fig. 3. At the given resolution, the new formulation

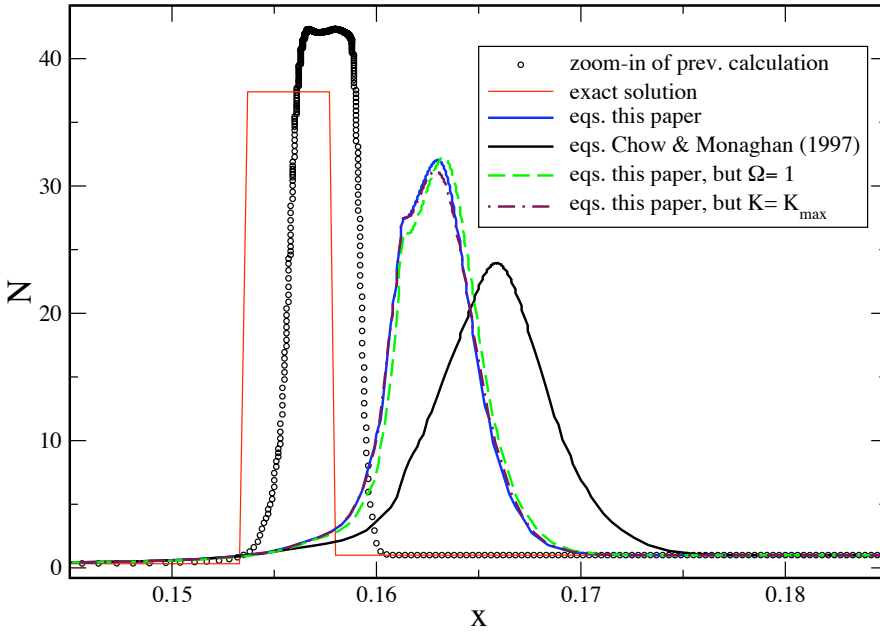


Fig. 4. Comparison between different formulations: exact solution (solid, red), zoom-in on the result of the calculation shown in Fig. 3 (circles), the suggested, new formulation (solid, blue), new formulation, but $\Omega = 1$ (dashed, green), new formulation, but $K = K_{\max} = 0.5$ (dot-dashed, maroon) and the original formulation [7] (solid, black).

(blue) performs best, but the differences between either keeping the dissipation constant (dot-dashed line) or setting $\Omega = 1$ (dashed, green) are small. All of them show a substantially higher peak density value and a significantly smaller shock-velocity excess than the reference formulation. This comparison suggests that the main difference comes again from using a different prescription for the signal velocity, the other modifications are negligible in comparison. The “grad-h”-terms slightly reduce the shock front velocity, but also lead to small overshoots (near $x \approx -0.15$ and 0.15) which are absent in the $\Omega = 1$ case.

4.3 Test 3: sinusoidally perturbed shock tube

Following [9], we explore a shock tube test whose initial right density state is sinusoidally perturbed:

$$(N, v, P)^L = (5, 0, 50) \quad \text{and} \quad (N, v, P)^R = (2 + 0.3 \sin(50x), 0, 5). \quad (50)$$

The main goal of this experiment is to test the ability to transport smooth structures across discontinuities. For this relatively mild shock only a moderate amount of dissipation is required, we use $K_{\max} = 0.2$. The numerical result at $t = 0.35$ is displayed in Fig. 5 together with the exact solutions of unperturbed shock tubes, once with a right hand side density value of 2.3 (dashed red line) and once with 1.7 (solid red line). Note the slightly larger shock speed in the latter case ($\gamma_{1.7} \approx 1.151$ vs. $\gamma_{2.3} \approx 1.149$). The numerical solution accurately reaches the correct levels of the limiting solutions in the shocked shell.

We perform the following test runs (400 particles between 0 and 1): i) the new

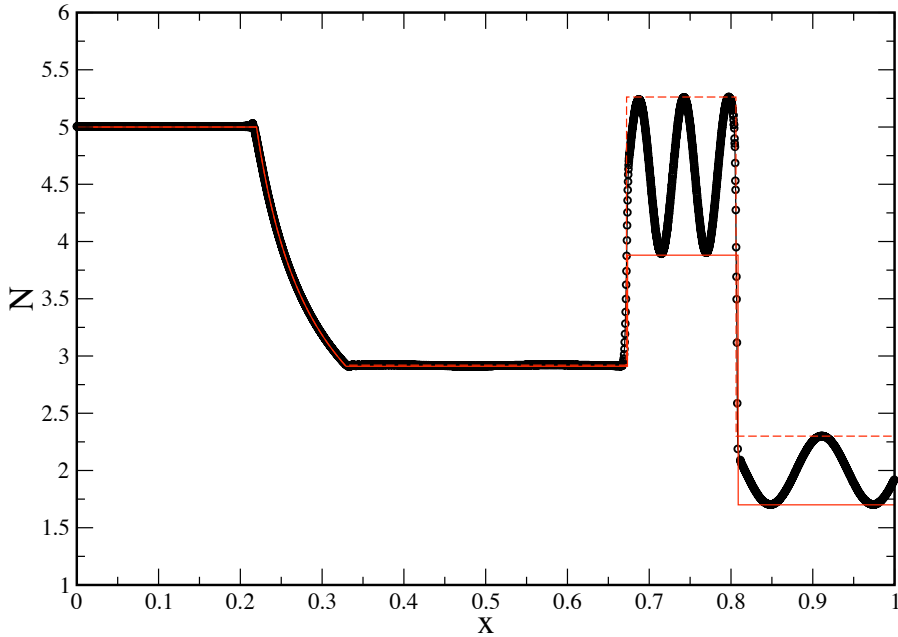


Fig. 5. Shock tube test where a relativistic shock propagates into a sinusoidally perturbed medium [9]. The SPH solution is shown as black circles, the red lines indicate the exact solutions for unperturbed right hand side densities of 1.7 (solid) and 2.3 (dashed).

equation set, ii) the reference equation set of Chow and Monaghan [7] iii) the

new equation set, but $\Omega = 1$ and iv) the new equation set, but $K = K_{\max}$. For a fair comparison with [7] we use $K_{\max} = 0.5$ in the tests. *All* of the variants could be substantially improved by using a lower value of K_{\max} . A zoom-in into the shocked shell is shown in Fig. 6 for all used variants. The conclusions are similar to the previous tests: the effects of the “grad-h-terms” are visible, but small, the effects of the time-dependent viscosity parameters (blue vs. maroon) and most importantly the different signal velocity (new vs. reference formulation) are substantially more important. These tendencies are found in all tests, we therefore only show the results from the new equation set in the subsequent numerical experiments.

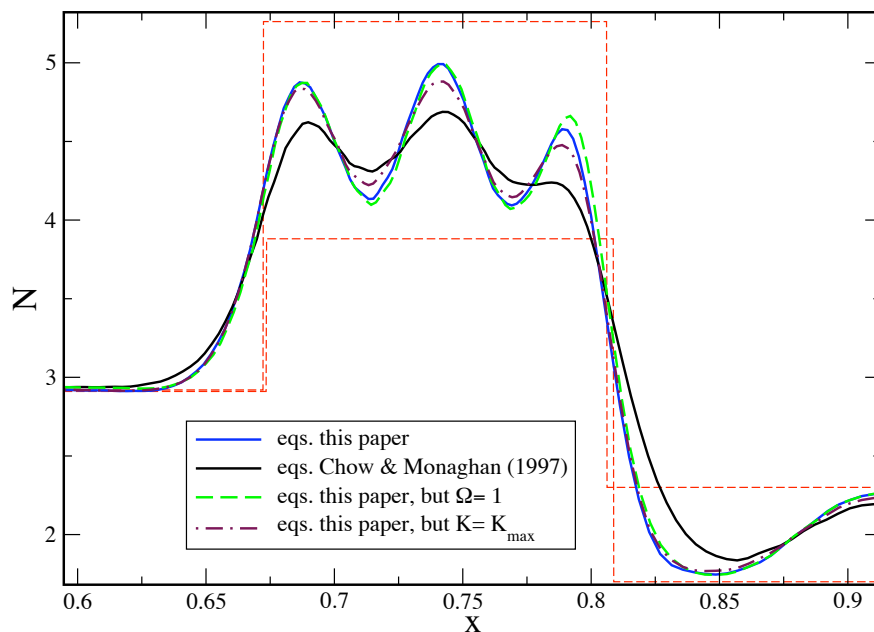


Fig. 6. Perturbed shock tube test, comparison of the different effects at low resolution: new formulation (solid, blue), new formulation, but $\Omega = 1$ (dashed, green), new formulation, but $K = K_{\max} = 0.5$ (dot-dashed, maroon) and the original formulation [7] (solid, black).

4.4 Test 4: Ultra-relativistic wall shock

In this test cold gas moves relativistically towards a wall. Upon hitting the wall a shock front forms that travels upstream against the inflowing gas leaving behind a hot and dense post-shock region with zero velocity. In the ultra-relativistic limit ($v \rightarrow 1$) the shock travels at $v_{\text{shock}} = -(\Gamma - 1)$, i.e. $v_{\text{shock}} =$

1/3 for the polytropic exponent $\Gamma = 4/3$ that we use in this test. The post-shock values of density, pressure and specific energy are $N_p = \Gamma/(\Gamma - 1)N_i$, $P_p = \gamma\Gamma N_i$, $u_p = \gamma$, where N_i is the initial density.

We model the reflecting wall as “ghost” particles streaming with opposite velocity from the right towards the wall located at $x = 1$. For this extremely strong shock we use $K_{\max} = 1$. For the initial gas velocity we use a value as high as $v = 0.9999999998$ corresponding to a Lorentz factor of 50 000! We further use $N_i = 1$ and a specific energy of $u_i = 10^{-5}$. The results of the numerical calculation (1000 particles) at $t=1$ are shown together with the ultra-relativistic limit values in Fig. 7. The agreement between the numerical

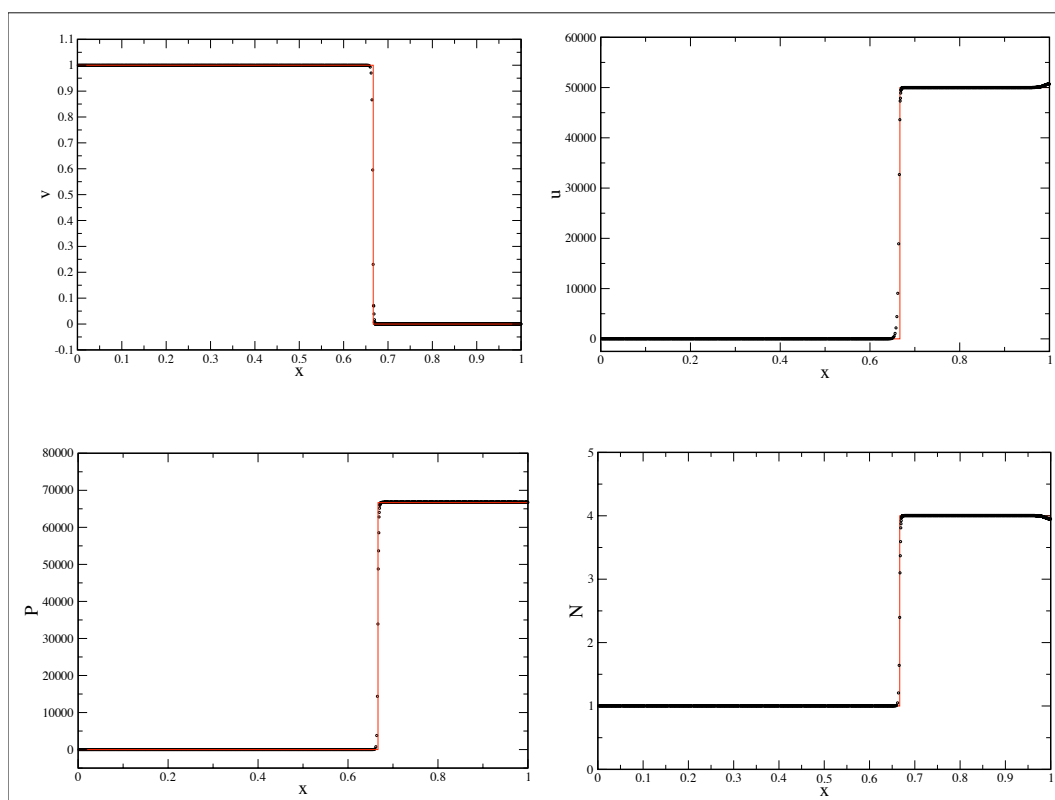


Fig. 7. Ultra-relativistic wall shock test: an ultra-relativistic, cold fluid with $(N, v, u) = (1, 0.9999999998, 10^{-5})$ moves towards a reflecting wall at $x=1$. Note that the initial velocity corresponds to a Lorentz factor as large as $\gamma = 50000$. The SPH result is shown as black circles, the exact result in the ultra-relativistic limit as red lines.

and the exact result is excellent, only the density and the specific energy show minor deviations from the exact solution (maximum error in density 1.2 %, in specific energy 1.1%) as a result of so-called “wall-heating” [34] near the boundary at $x=1$.

4.5 Test 5: Relativistic advection of a sine wave

In this test we explore the ability to accurately advect a smooth density pattern. We choose a sine wave that propagates towards the right through a periodic box. Since this test does not involve shocks, we switch off the artificial dissipation terms. We use 500 aequidistantly placed SPH particles in the interval $[0,1]$, enforce periodic boundary conditions and use a polytropic equation of state with $\Gamma = 4/3$. We impose a computing frame number density $N(x) = N_0 + \frac{1}{2} \sin(2\pi x)$, a constant velocity $v_0 = 0.997$ corresponding to a Lorentz factor $\gamma \approx 12.92$ and we instantiate a constant pressure corresponding to $P_0 = (\Gamma - 1)n_0u_0$, where $n_0 = N_0/\gamma$, $N_0 = 1$ and $u_0 = 1$. The specific energies of the particles are chosen so that each particle has the same pressure P_0 .

The advection of this relativistic sine wave is essentially perfect, see Fig. 8: the result after as many as 100 box crossings (circles) is indistinguishable from the initial setup (red line), neither wave amplitude nor phase have been noticeably affected during the evolution.

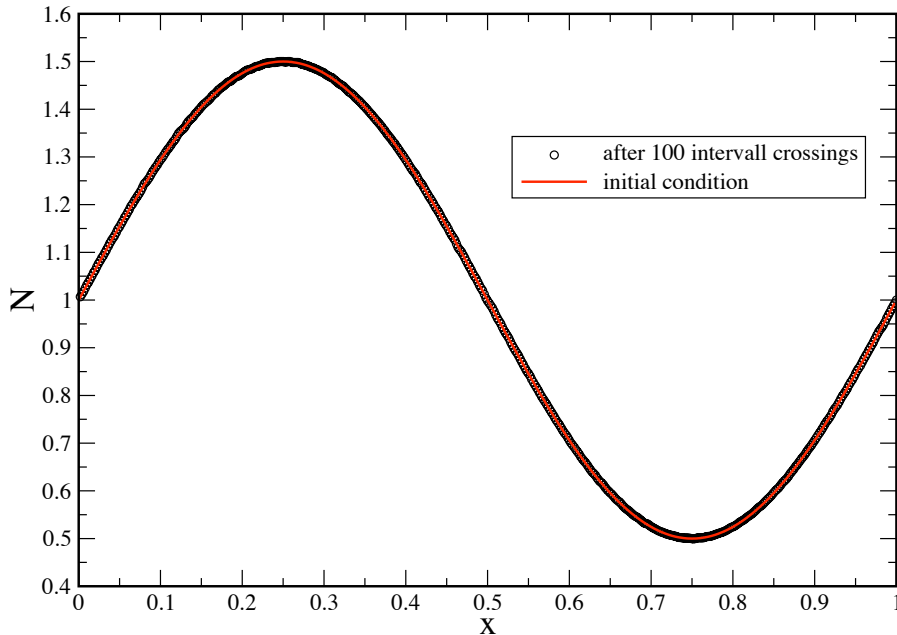


Fig. 8. Advection of a relativistically moving sine wave (Lorentz factor $\gamma \approx 12.92$) across a periodic box: the initial condition of the computing frame number density, N , is shown as solid, red line, the result after as many as 100 box crossings is overplotted as circles.

4.6 Test 6: Relativistic advection of a square wave

In this test we advect a square wave through the interval $[0,1]$, again using periodic boundaries. Due to the involved steep flanks this problem is substantially more challenging than the previous one. We represent our box-shaped number density profile, $N(x)$, numerically as the sum of two Fermi-functions transiting from a lower state N_{low} at x_1 to a higher state, N_{high} , and back to the lower state at x_2 :

$$N(x) = N_{\text{low}} + (N_{\text{high}} - N_{\text{low}}) \left\{ \frac{1}{1 + \exp(\frac{x-x_2}{\Delta x})} - \frac{1}{1 + \exp(\frac{x-x_1}{\Delta x})} \right\}, \quad (51)$$

where Δx sets the length scale on which the transitions occur. For the numerical experiments, we use $N_{\text{low}} = 1.0$, $N_{\text{high}} = 1.1$ and Δx is set to twice the particle spacing in the low density region. We use equal mass particles in this test, constant pressure throughout the box is instantiated as in the sine wave problem above and we impose again a constant initial velocity of $v_0 = 0.997$. The results are displayed in Fig. 9: the black circles show the initial number density profile, the results after 5 and 10 box crossings are shown as red circles and blue triangles, respectively. Overall the results of this challenging test agree very well with the initial state, but after 10 box crossings the flanks have slightly softened, and the low density state close to the flanks has been slightly increased.

4.7 Test 7: Evolution of a relativistic simple wave

Here we present results of a challenging test that involves relativistic simple waves and is rarely shown in the literature.

Relativistic simple waves [42,12,19,2,1] are characterized by the spatial and temporal constancy of two of the three Riemann invariants for one dimensional fluid flows. The three Riemann invariants are the specific entropy, s , and the quantities

$$J_{\pm} = \ln(\gamma + U) \pm \int \frac{c_s}{\rho} d\rho, \quad (52)$$

where c_s is the sound speed and U the x-component of the four velocity. Simple waves propagating to the right/left are characterized by the constancy of s and J_-/J_+ . In this test, a purely compressive initial sine pulse is set up that propagates into a static, uniform medium. According to the results of [2], the initial velocity pulse will steepen while maintaining its peak velocity until it evolves into a relativistic strong shock with Mach number 2.65. From

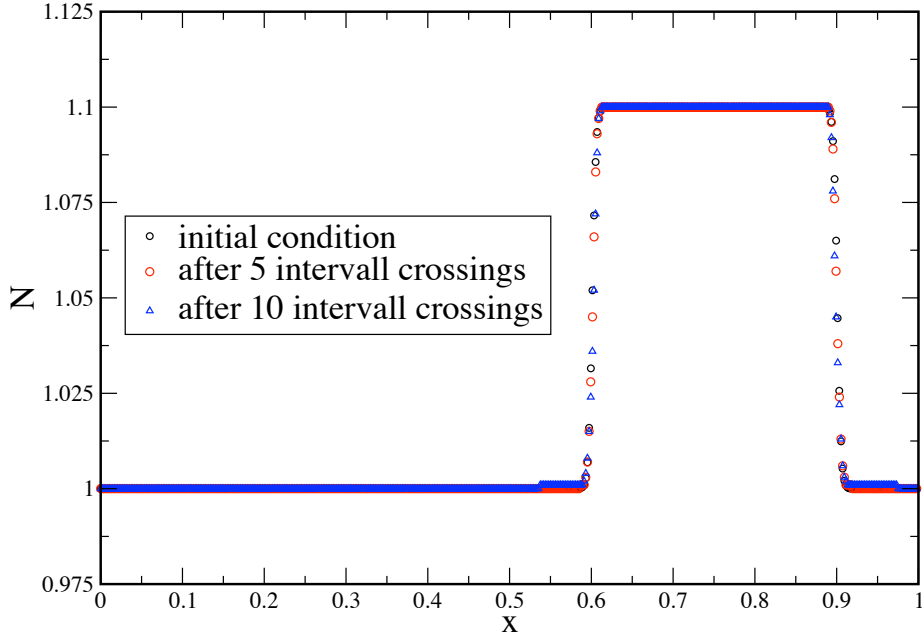


Fig. 9. Advection of a relativistically moving square wave (Lorentz factor $\gamma \approx 12.92$) across a periodic box: the initial condition of the computing frame number density, N , is shown as black circles, the result after 5 box crossing times (red circles) and 10 box crossing times (blue triangles) are overlotted.

thereon, the wave will dissipate and continuously decrease in velocity and in the contrasts of density and internal energy (as measured with respect to the initial unperturbed state).

Our setup and parameter choice closely follows [2]. We use the equation of state of a radiation-dominated fluid, $p = k(s)\rho^{4/3}$. The initial state consists of an unperturbed fluid state denoted by subscript 0 with an overlaid "velocity pulse". Like in [2], we choose the sound velocity in the unperturbed state as $c_0 = 0.3$ and display normalized, dimensionless quantities. For the initial (local rest frame) density we choose $n_0 = 1$ and we use the length of our initial velocity pulse, $l_0 = 100$, as characteristic length scale. The normalized quantities are denoted with a $\hat{\cdot}$ -symbol: $\hat{\mu} = \mu/(n_0 l_0)$, where μ is the mass coordinate, $\hat{n} = n/n_0$, $\hat{u} = u/u_0$, $\hat{s} = s/s_0$, $\hat{P} = P/P_0$ and $\hat{t} = t/l_0$. We proceed in the following steps:

- choose a sinusoidal velocity profile with a maximum $v_{\max} = 0.7$ as a function of $\hat{\mu}$. The width of the pulse in normalized mass coordinates is $\hat{\mu}_0 = \pi$. To keep the pulse sufficiently far away from the (fixed) boundaries particles (at $\hat{\mu} = 0$ and 13), we choose $\hat{\mu}_{\text{peak}} = 3$ as mass coordinate of the velocity

maximum. For the ease of comparison, we plot the results with a constant $\hat{\mu}$ -offset so that our initial setup (black curves in Fig. 10), coincides with the initial conditions of [2], see their Figure 5.

- Once v is known, we calculate the sound velocity [19,2] as a function of $\hat{\mu}$

$$c_s = \frac{\frac{1+c_0\sqrt{3}}{1-c_0\sqrt{3}} \left(\frac{1+v}{1-v} \right)^{\frac{1}{2\sqrt{3}}} - 1}{\sqrt{3} \left[\frac{1+c_0\sqrt{3}}{1-c_0\sqrt{3}} \left(\frac{1+v}{1-v} \right)^{\frac{1}{2\sqrt{3}}} + 1 \right]} \quad (53)$$

- and from this the specific energy and rest frame number density

$$u = \frac{9c_s^2}{4(1-3c_s^2)} \quad \text{and} \quad n = n_0 \left(\frac{u}{u_0} \right)^3. \quad (54)$$

- Finally, the computing frame baryon number density, $N = \gamma n$, is calculated which, in turn, allows to assign positions and baryon numbers.

We display in Fig. 10 v , $\delta n/n_0 = \hat{n} - 1$, $\delta u/u_0 = \hat{u} - 1$ and $\delta s/s_0 = \hat{s} - 1$, where the axis limits and output times are chosen as in Fig. 5 of [2]. The specific entropy is nowhere used in our SPH formulation, but can be post-processed for the chosen equation of state as $\hat{s} = \hat{P}^{3/4} \hat{n}^{-1}$.

Generally, we find very good agreement with the results of [2]. The initial sine-pulse continuously steepens while keeping its maximum velocity constant (to within about 2%) until a relativistic shock forms (at $\hat{t} \approx 1$), see Fig. 10 upper left. Note in particular that the positions of the shock fronts agree excellently with those found in [2]. The wave subsequently dissipates, thereby producing a double peak structure in the density contrast (at $\hat{t} = 1.09$, upper right) with the dip coinciding with the peak in the entropy (lower right) and the steep flank at $\hat{\mu} = 3.5$ in the specific energy (lower left). The entropy shows a small, spurious overshoot at the leading edge which is the result dividing $\hat{P}^{3/4}$ and \hat{n} at the shock front, but apart from this, the agreement with [2] is very good. We only find minor differences. Our simulations are less dissipative, the second density peak, for example, still exceeds the leading one at $\hat{t} = 1.09$ and is still visible at 7.40 while by the same time it has vanished in [2]. Moreover, our specific energy at $\hat{t} = 1.09$ shows a clear plateau behind the shock while theirs is a very smooth peak (which may just be the result of lower resolution), and our entropy peak (at $\hat{\mu} \approx 3.75$) is slightly smaller than theirs ($\delta s/s_0 = 0.61$ vs. ≈ 0.67).

5 Summary

We have derived a new set of special-relativistic SPH equations from a variational principle. This work differs from [31] in that it includes also the special-

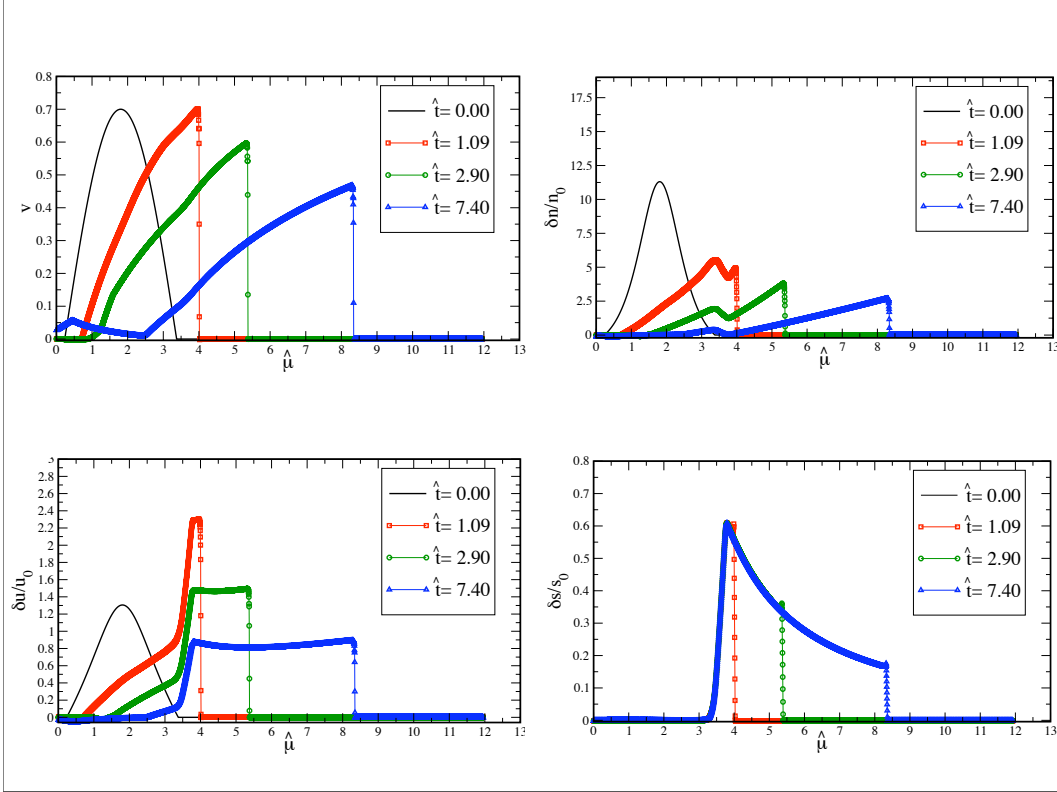


Fig. 10. Evolution of a relativistic simple wave: starting from a velocity sine pulse propagating to the right into a uniform medium, a shock forms that subsequently dissipates the wave. Shown are the velocity (upper left), and the contrasts in (rest frame) density (upper right), specific energy (lower left) and entropy (lower right).

relativistic “grad-h” terms that account for derivatives of the smoothing kernels with respect to the resolution lengths. We have used an artificial viscosity prescription that is inspired by analogy to Riemann solvers, similar to the one suggested in [28]. We have introduced a new form for the signal velocity and we restrict the effect of the artificial viscosity to regions where it is required. This is achieved via time-dependent viscosity parameters which are obtained by solving an additional differential equation similar to the non-relativistic approach suggested by [32].

We have carefully tested this new approach in a slew of numerical benchmark tests. We find that the relativistic grad-h terms increase the accuracy of the results, but usually only have a minor effect. The improvements are generally dominated by the new signal velocity and the time-dependent viscosity parameters. The new approach yields excellent results in the numerical experiments. As expected for a purely Lagrangian scheme, it performs very well in pure advection problems, even at large Lorentz factors, see test problems 5 and 6. What is more, it also yields accurate results even in very strong shock tests, which are usually considered a particular challenge for SPH. For example, the scheme is able to accurately handle wall shock problems with a Lorentz factor as large as $\gamma = 50000$, see test 4. We also perform a challenging test in which

a relativistic simple wave steepens into a strong shock and subsequently dissipates. Our numerical results for this test are in close agreement with those obtained by [2].

Previous SPH formulations have turned out to carry over in a straight forward manner to higher dimensions, this generalization of our scheme is left to future investigations.

Acknowledgements It is a pleasure to thank SISSA (Trieste, Italy) and in particular John Miller for warm hospitality and many insightful discussions. This work has been supported by DFG under grant RO 3399/5-1.

References

- [1] A. M. Anile, *Relativistic fluids and magneto-fluids*, Cambridge Monographs on Mathematical Physics, Cambridge University Press, 1989.
- [2] A. M. Anile, J. C. Miller, S. Motta, Formation and damping of relativistic strong shocks, *Physics of Fluids* 26 (1983) 1450–1460.
- [3] P. Anninos, P. C. Fragile, Nonoscillatory Central Difference and Artificial Viscosity Schemes for Relativistic Hydrodynamics, *ApJS* 144 (2003) 243–257.
- [4] W. Benz, Smooth particle hydrodynamics: A review, in: J. Buchler (ed.), *Numerical Modeling of Stellar Pulsations*, Kluwer Academic Publishers, Dordrecht, 1990, p. 269.
- [5] L. Brookshaw, A method of calculating radiative heat diffusion in particle simulations, *Proceedings of the Astronomical Society of Australia* 6 (1985) 207–210.
- [6] A. Celotti, G. Ghisellini, M. Chiaberge, Large-scale jets in active galactic nuclei: multiwavelength mapping, *MNRAS* 321 (2001) L1–L5.
- [7] J. E. Chow, J. Monaghan, Ultrarelativistic sph, *J. Computat. Phys.* 134 (1997) 296.
- [8] L. Del Zanna, N. Bucciantini, An efficient shock-capturing central-type scheme for multidimensional relativistic flows. I. Hydrodynamics, *A&A* 390 (2002) 1177–1186.
- [9] A. Dolezal, S. S. M. Wong, , *J. Comp. Phys.* 120 (1995) 266.
- [10] R. Donat, A Flux-Split Algorithm Applied to Relativistic Flows, *Journal of Computational Physics* 146 (1998) 58–81.
- [11] M. R. Dubal, Numerical simulations of special relativistic, magnetic gas flows, *Computer Physics Communications* 64 (1991) 221–234.
- [12] P. G. Eltgroth, Similarity Analysis for Relativistic Flow in One Dimension, *Physics of Fluids* 14 (1971) 2631–2635.

- [13] S. A. E. G. Falle, S. S. Komissarov, An upwind numerical scheme for relativistic hydrodynamics with a general equation of state, *MNRAS* 278 (1996) 586–602.
- [14] V. Fock, *Theory of Space, Time and Gravitation*, Pergamon, Oxford, 1964.
- [15] Y. A. Gallant, J. Arons, Structure of relativistic shocks in pulsar winds: A model of the wisps in the Crab Nebula, *ApJ* 435 (1994) 230–260.
- [16] R. A. Gingold, J. J. Monaghan, Smoothed particle hydrodynamics - Theory and application to non-spherical stars, *MNRAS* 181 (1977) 375–389.
- [17] A. Kheifets, W. A. Miller, W. H. Zurek, Covariant smoothed particle hydrodynamics on a curved background, *Physical Review D* 41 (1990) 451–454.
- [18] P. Laguna, W. A. Miller, W. H. Zurek, Smoothed particle hydrodynamics near a black hole, *ApJ* 404 (1993) 678–685.
- [19] E. P. T. Liang, Relativistic simple waves - Shock damping and entropy production, *ApJ* 211 (1977) 361–376.
- [20] L. Lucy, A numerical approach to the testing of the fission hypothesis, *The Astronomical Journal* 82 (1977) 1013.
- [21] P. Mann, A relativistic smoothed particle hydrodynamics method tested with the shock tube, *Computer Physics Communications*.
- [22] P. Mann, Smoothed particle hydrodynamics applied to relativistic spherical collapse, *Journal of Computational Physics* 107 (1993) 188–198.
- [23] A. Marquina, J. M. Martí, J. M. Ibanez, J. A. Miralles, R. Donat, Ultrarelativistic hydrodynamics - High-resolution shock-capturing methods, *A & A* 258 (1992) 566–571.
- [24] J. Martí, J. Ibanez, J. Miralles, *Phys. Rev. D* 43 (1991) 3794.
- [25] J. Martí, E. Müller, *J. Comp. Phys.* 123 (1996) 1.
- [26] J. M. Martí, E. Müller, *Numerical Hydrodynamics in Special Relativity*, *Living Reviews in Relativity* 6 (2003) 7.
- [27] J. J. Monaghan, Smoothed particle hydrodynamics, *Ann. Rev. Astron. Astrophys.* 30 (1992) 543.
- [28] J. J. Monaghan, SPH and Riemann Solvers, *Journal of Computational Physics* 136 (1997) 298–307.
- [29] J. J. Monaghan, SPH compressible turbulence, *MNRAS* 335 (2002) 843–852.
- [30] J. J. Monaghan, Smoothed particle hydrodynamics, *Reports on Progress in Physics* 68 (2005) 1703–1759.
- [31] J. J. Monaghan, D. J. Price, Variational principles for relativistic smoothed particle hydrodynamics, *MNRAS* 328 (2001) 381–392.

- [32] J. Morris, J. Monaghan, A switch to reduce sph viscosity, *J. Comp. Phys.* 136 (1997) 41.
- [33] R. Nelson, J. Papaloizou, Variable smoothing lengths and energy conservation in smooth particle hydrodynamics, *MNRAS* 270 (1994) 1.
- [34] M. L. Norman, K.-H. Winkler, Why ultrarelativistic numerical hydrodynamics is difficult, in: K.-H. Winkler, M. L. Norman (eds.), *Astrophysical Radiation Hydrodynamics*, Reidel, Berlin, 1986.
- [35] T. Piran, The physics of gamma-ray bursts, *Reviews of Modern Physics* 76 (2005) 1143.
- [36] D. Price, Magnetic fields in astrophysics, Ph.D. thesis, University of Cambridge, arXiv:astro-ph/0507472 (2004).
- [37] S. Rosswog, Astrophysical smooth particle hydrodynamics, *New Astronomy Reviews*.
- [38] S. Rosswog, D. Price, Magma: a magnetohydrodynamics code for merger applications, *MNRAS* 379 (2007) 915 – 931.
- [39] S. Siegler, Entwicklung und untersuchung eines smoothed particle hydrodynamics verfahrens für relativistische strömungen, Ph.D. thesis, Eberhard-Karls-Universität Tübingen (2000).
- [40] S. Siegler, H. Riffert, Smoothed Particle Hydrodynamics Simulations of Ultrarelativistic Shocks with Artificial Viscosity, *ApJ* 531 (2000) 1053–1066.
- [41] V. Springel, L. Hernquist, Cosmological smoothed particle hydrodynamics simulations: the entropy equation, *MNRAS* 333 (2002) 649–664.
- [42] A. H. Taub, Relativistic Rankine-Hugoniot Equations, *Physical Review* 74 (1948) 328–334.
- [43] L. Wen, A. Panaitescu, P. Laguna, A Shock-patching Code for Ultrarelativistic Fluid Flows, *ApJ* 486 (1997) 919–+.